Transition from correlated to single-active-electron excitation in strontium nonlinear ionization

A. Dimitriou, V. Loriot, A. Marciniak, T. Barillot, S. Danakas, F. Lépine, C. Bordas, S. Cohen

Transition from correlated to single-active electron excitation in strontium nonlinear ionization

A. Dimitriou[1*], V. Loriot[2], A. Marciniak[2], T. Barillot[2], S. Danakas[1], F. Lépine[2], C. Bordas[2] and S. Cohen[1†]

[1]*Atomic and Molecular Physics Laboratory, Physics Department, University of Ioannina, 45110 Ioannina, Greece*

[2]*Université de Lyon, CNRS, UMR5306, Institut Lumière Matière, 69622 Villeurbanne, France*

Abstract

The nonlinear single and double ionization of Sr atoms as a result of their interaction with 800 nm Ti-Sapphire laser pulses of 25 fs duration is experimentally investigated within the laser intensity range I = 3 TWcm^{-2} - 30 TWcm^{-2}. The latter range includes the over-the-barrier intensities for both Sr and Sr^{+}, while the corresponding Keldysh adiabaticity parameters are larger than unity. Nevertheless, for $I\geq$24 TWcm^{-2} the recorded photoelectron energy spectra show evidence of the (partial) applicability of tunneling or over-the-barrier ionization concepts, whereas below this value they can be discussed in terms of multiphoton ionization processes. More importantly, the data additionally point towards a further division of the multiphoton regime into two sub-ranges separated roughly at I ~ 4 TWcm^{-2}. Above this value above-threshold-ionization structures and the single-active-electron picture dominate. On the contrary, at the lowest laser intensities the photoelectron spectra and angular distributions reveal single ionization pathways where the remaining ion is left into excited states. These pathways also require photon absorption in the continuum, which in the case of strontium and other alkaline earth atoms is structured by the presence of doubly excited states which are embedded in it. Hence, in this case ionization proceeds via quasi-resonant ionization ladders formed by these doubly excited states which are dominated by the interaction between the two valence electrons of Sr. We discuss in detail the above rich phenomenology and relevant ionization mechanisms and propose possible directions of further work towards the elucidation of the role of configuration interaction in ionization processes.

PACS numbers: 32.80.Fb, 32.80.Rm, 33.60.-q, 32.80.Dz

† Corresponding author: scohen@uoi.gr

I. INTRODUCTION

The nonlinear (single, double or even multiple) ionization of multi-electron atoms is a subject of high interest in photophysics as it questions the nature of electron correlation. Early investigations in intense laser-atom interaction concerned alkaline earth metal atoms [1,2,3,4,5,6,7,8,9,10,11,12] ionized by long laser pulses (~ns or ~ps) at moderate intensity (≤10 TWcm^{-2}). They were soon followed by experiments on noble gases [13], the latter offering much higher ionization limits that are capable of withstanding higher laser intensities available with ultrashort (~fs) laser pulses. With the emergence of strong field atomic physics, non-linear ionization was categorized with the help of simple concepts such as the Keldysh adiabaticity parameter [14] $\gamma = [IP/(2U_p)]^{1/2}$, expressed via the target's ionization potential IP and the ponderomotive energy $U_p = I/4\omega^2$ (in atomic units) of the laser field of frequency ω and intensity I [15]. According to such a categorization, the condition $\gamma > 1$ characterizes the perturbative multi-photon ionization (MPI) regime leading to above-threshold ionization (ATI) [16]. In ATI the ionized electron absorbs photons in excess of the minimum number required to overcome the ionization threshold. On the other hand the condition $\gamma<1$ is fulfilled at higher laser intensity and characterizes the non-perturbative tunnel ionization regime [15]. Further increase of the intensity leads to over-the-barrier ionization (OBI) [15], where above a critical intensity I_{OBI} the light field completely suppresses the Coulomb barrier. In fact, this simple description is often insufficient because the non-homogenous spatiotemporal distribution of the laser intensity may mix the different regimes [17]. It is to be further emphasized that the above description relies essentially on a single-active-electron picture [18]. Within this latter context, alkali metal atoms having a single valence electron outside closed subshells were recently used as model target systems [19,20,21,22,23,24,25,26,27]. For these low IP atoms I_{OBI} is sufficiently low and leads to $\gamma(I_{\mathrm{OBI}})>1$. Surprisingly, under such an apparently conflicting condition the ionization of these systems could be perfectly described in terms of MPI [20,25].

Alkaline earth metal atoms are also low IP systems having two valence electrons outside a closed-subshell ionic core (ground state configurations […]n_gs^2, where […] denotes the core). Thus, they appear to be suitable for studying the role of multielectron effects which are at play in nonlinear ionization. Indeed, earlier long-pulse and low-intensity investigations [5,7,9,10,11,12] already pointed out that the single-active-electron assumption is frequently invalid for these systems. Excitation of the two valence electrons results in dense manifolds of doubly excited states located near their first […]n_gs ionization thresholds and all the way up to their double ionization limits. These states were found to act as resonant or near-resonant intermediate levels and form excitation ladders that led to the absorption of a number of photons within the (structured) continuum. This process differs qualitatively from the single-active-electron ATI process mentioned earlier. In

addition, ionization via such ladder schemes was found to create populations of *excited* states of the singly charged ions [5]. This effect constitutes a typical signature of the interaction between the two valence electrons and the consequent extensive configuration interaction (CI) and mixing between (quasi-discrete and continuum) doubly excited configurations [28]. Despite this fact, "direct" two electron ejection was never evidenced in alkaline earths under these conditions. Nevertheless, the production of excited ionic level populations facilitated their sequential double ionization where atoms are ionized first and the resulting singly charged ions are further ionized within the same laser pulse [1-12].

Until recently nonlinear ionization of alkaline earths using ultrashort and intense fs pulses was rather rarely investigated (either theoretically [29,30,31] or experimentally [32,33,34,35,36]) with a particular focus on the Mg atom. Indeed, the first ionization threshold of Mg (≈7.6 eV) was anticipated to be sufficiently high for allowing a meaningful comparison with the results of short pulse nonlinear ionization experiments in noble gas [33]. The measured ATI electron spectra in Mg could be interpreted in terms of single-active-electron ionization, while a weaker ATI series originating from CI-driven ionization and leaving the ion to its excited 3p state was unfortunately blended with the sequential double ionization signal [32]. Further investigations concerned the resonant structures exhibited by the ATI peaks [35] and the non-sequential double ionization [34]. More recently, ionization induced by recollision processes was investigated at longer wavelength (1-2 μm) [37,38,39] in Mg and heavier alkaline earth atoms. The general conclusion drawn from these studies is that non-sequential double ionization proceeds via the excited ionic states which are pumped by the impact of the returning electron, but the atom-specific doubly excited spectrum does not seem to play any role. Consequently, the implication of these CI-mediated states to the overall laser induced dynamics throughout from MPI to OBI still remains an open issue requiring further study.

The purpose of the present work is to shed more light on the above issue, by investigating the nonlinear single and double ionization of Sr using intense ≈800 nm and ≈25 fs laser pulses and a velocity-map imaging spectrometer (VMIS). Strontium atom is chosen because earlier long-pulse studies showed that CI-mediated above-threshold ionization is much stronger for it [10,11,12] as compared to other alkaline earths atoms [7,9] under similar excitation conditions. The recorded photoelectron energy spectra (PES) and photoelectron angular distributions (PADs) show indeed such evidence. However, as the laser intensity is increased we first observe a transition towards single-active-electron ATI structures and as it is increased even more we observe another transition towards the tunneling regime onset. Although this is a byproduct of our principal investigation, the latter MPI-to-tunneling ionization transition is also discussed here in connection with the aforementioned recent studies in alkali atoms under conflicting conditions. These results offer new

perspectives for studying electron-correlation in the ultrafast regime and may prove useful for putting into stringent test future relevant theoretical models.

II. EXPERIMENTAL SETUP AND PROCEDURE

The experimental set-up consists of two differentially-pumped vacuum chambers connected via an electronically controlled valve. The first chamber encloses an electrically heated stainless steel oven filled with strontium pellets and heated to ≈550 °C. The produced Sr vapor passes through a 0.5 mm diameter hole and forms a thermal atomic beam entering to the second chamber when the valve is open. This laser-atom interaction chamber is pumped by a 250 l/s turbomolecular pump – rotary pump system maintaining a background pressure of $\sim 10^{-7}$ mbar.

Strontium atoms interact with laser radiation delivered by a Ti: Sapphire laser (Coherent, Legend Elite Duo USX) producing pulses of ≈800 nm central wavelength, ≈52 nm bandwidth and ≈25 fs pulse duration, while operating at 5 kHz repetition rate. The linearly polarized laser beam emerging from this system passes through an assembly composed of an achromatic half-wave plate and a (dielectric thin-film multilayer) linear polarizer for setting its polarization parallel to the electron detector plane (see below) and for intensity control. Subsequently the beam is focused into the interaction region by a 25 cm focal length lens.

The atomic and laser beams are perpendicular to each other, as well as to the axis of the VMIS. The latter is based on a standard three-electrode design [40], where photoionization takes place in the center between a solid repeller plate and an extractor plate 20 mm apart and with a 20-mm central hole. These electrodes are followed by an equally spaced grounded third electrode identical to the extractor plate. Typically, electrode voltages are $V_{\mathrm{Rep}} \approx -3.5$ kV and $V_{\mathrm{Ext}} \approx -2.5$ kV, in order to ensure proper VMIS focusing conditions [40,41]. The electric field created by the three electrodes accelerates photoelectrons towards the end of a 15 cm long field-free drift tube where they are detected by a two-dimensional position-sensitive detector. The latter is made of a tandem Hamamatsu F2225-21P microchannel plate (MCP) assembly and a P42 phosphor screen. The entire spectrometer is shielded against parasitic magnetic fields by means of a double μ-metal layer. A CCD camera (Allied Vision, Marlin F146B) records the 2D distribution of light spots on the screen. Recorded images are transferred to a PC, where they are accumulated over several hundred thousand laser shots.

The processing of raw images is performed off-line. The PES and PADs are obtained from the recorded 2D projections. For cross-checking purposes we employed two inversion procedures based on the Vrakking's method [42] and the so-called Polar Onion Peeling one [43]. Both methods produced identical results within experimental resolution and the PADs presented in this work are

those obtained by Vrakking's method. Electron energy calibration is achieved via the observed ATI electron peaks. Judging from the measured smallest energy difference between closely spaced electron peaks and their widths, the resolution of the spectrometer is better than ≈0.1 eV for electron energies of the order of 1 eV. As for the detection of produced ions, it is achieved by simply reversing the polarities of the voltages applied to the interaction-region-electrodes of the VMIS and operating the instrument as a simple ion time-of-flight mass spectrometer. Finally, the laser beam intensity calibration is accomplished by employing this ion detection operating mode and measuring the ratio between the single and double ionization yield of Xe [44] in a separate study. We estimate that our reported laser intensities are accurate to within 10%.

III. EXCITATION AND IONIZATION PATHWAYS

Before presenting our experimental data it will be helpful to discuss first the relevant excitation and ionization pathways. These are schematically shown in the scaled (though partial) energy level diagram of Fig. 1 without considering any ponderomotive and/or dynamic (AC) Stark level shifts. We initially restrict ourselves to the processes where the atom, initially in its $5s^2\ ^1S_0$ ground state, absorbs a number of photons and ionizes, leaving the singly charged ion to a given $n_i\ell_i$ level. By assuming strictly non-resonant ionization conditions and that the atomic $5s^2$ ground state is AC Stark shifted by ΔE_{5s^2} while the $n_i\ell_i$ limit $IP_{n_i\ell_i}$ is shifted by U_p [45], the kinetic energy of the electron released by such a process may be approximated by,

$$\varepsilon_{n_i\ell_i,N} = N\omega - IP_{n_i\ell_i} - (U_p - \Delta E_{5s^2}). \quad (1)$$

Just like the ponderomotive energy (given by $U_p(\text{eV}) = 5.95\times10^{-2} I\ (\text{TWcm}^{-2})$ for the wavelength employed here), the quantity ΔE_{5s^2} is expected to vary linearly with laser intensity I. As for the integer N, it stands for the total number of absorbed photons out of the ground state,

$$N = N_{n_i\ell_i} + k, \quad k=0,1,2,\ldots \quad (2)$$

where $N_{n_i\ell_i}$ is the minimum number required to ionize the atom with respect to the $n_i\ell_i$ threshold and integer k describes the ATI process associated with this threshold. To facilitate our discussion we label the above described process as $n_i\ell_i(k)$ and the pathways that are or could be of relevance to the present work are summarized in the following equations (3)-(9), most of them drawn also in Fig. 1:

$$5s(k): \quad Sr(5s^2) + (4 + k)\omega \rightarrow Sr^+(5s) + e\ (0.51\ \text{eV} + k\omega) \quad (3)$$

$$4d(k): \quad Sr(5s^2) + (5 + k)\omega \rightarrow Sr^+(4d) + e\ (0.23\ \text{eV} + k\omega) \quad (4)$$

$$5p_j(k): \quad Sr(5s^2) + (6 + k)\omega \rightarrow Sr^+(5p_j) + e\ (0.57(j=3/2)/0.67(j=1/2)\ \text{eV} + k\omega) \quad (5)$$

$$6s(k): \quad Sr(5s^2) + (8 + k)\omega \rightarrow Sr^+(6s) + e\ (0.79\ \text{eV} + k\omega) \quad (6)$$

$$6p(k): \quad Sr(5s^2) + (9 + k)\omega \rightarrow Sr^+(6p) + e\ (1.32\ \text{eV} + k\omega) \quad (7)$$

$$4f(k): \quad Sr(5s^2) + (9 + k)\omega \rightarrow Sr^+(4f) + e\ (0.69\ eV + k\omega) \tag{8}$$

$$7s(k): \quad Sr(5s^2) + (9 + k)\omega \rightarrow Sr^+(7s) + e\ (0.20\ eV + k\omega) \tag{9}$$

where $\omega \approx 1.55$ eV. The process corresponding to Eq. (5) is denoted as $5p_j(k)$ and the ≈0.1 eV spin-orbit splitting is taken into account because it is comparable to the energy resolution of our spectrometer. Note further that the $k = 0$ electron energies reported in the above equations were computed without considering any kind of shift. If U_p and ΔE_{5s^2} are considered in Eq. (1), the above given electron energies decrease linearly with I and Fig. 1 turns out to be somewhat misleading. For example, by ignoring ΔE_{5s^2} to a first approximation, Eq. (1) predicts that for the lowest intensity employed here the 5d(0) channel [$Sr(5s^2) + 8\omega \rightarrow Sr^+(5d) + e$] is expected to be *closed*, that is, $\varepsilon_{5d,8}(I) \leq 0$ [45]. For this reason we do not consider this process in the above equations. In addition, for the same intensity the 4d(0) and 7s(0) channels are about to be closed. It should be stressed, however, that high-lying $[\ldots]n_i\ell_i n\ell$ series of Rydberg states and the $n_i\ell_i$ thresholds these series converge to are expected to suffer (approximately) the same U_p shift. This circumstance has two consequences. First, even above the channel closing intensity these excited levels may sustain ionization by gradually upshifting to resonance within the time development of the laser pulse (the so-called Freeman resonances [46]). Second, either below or above the closing intensity the energies of electron peaks corresponding to Freeman resonances are approximately independent of I. Then Eq. (1) is invalid and the initial level AC Stark shift and U_p may solely affect the threshold intensity where the resonance condition is satisfied.

Leaving aside the missing shifts, the atomic ionization pathways of Fig. 1 are drawn in a way that allows their broad classification into typical ATI processes and non-typical absorption in the structured continuum. Consider, for example, the $5s(k>0)$ pathway belonging to the former category, where one optically-active electron absorbs photons above the first ionization threshold. Then, ionization occurs with a certain probability at each absorption step, while the singly charged ion is always left unexcited, that is the 5s ground state electron is a spectator. In other words, this ATI channel involves only $5s\varepsilon\ell$ atomic continuum configurations, with ε and ℓ determined by energy conservation and angular momentum dipole selection rules, respectively (recall that absorption of linearly polarized radiation obeys the $\Delta m_J = 0$, $\Delta J = \pm 1$ and parity change dipole selection rules per each absorbed photon).

Consider next those processes where atomic MPI results in an excited singly charged ion, as described by Eqs. (4)-(9). This mechanism strongly depends on the existence of energy level structure in the energy ranges reached after absorption of m photons from the atomic ground state (m=1,2,3, etc.) and, therefore, its understanding requires the examination of this structure first. Let us begin by noting that there are no resonant or near-resonant states at the first and second photon level [47,48]. On the contrary, by taking into account the *effective* three-photon laser bandwidth [49]

we find the 4d5p $^1F_3$ and 5s7p $^1P_1$ three-photon near-resonant states, both lying slightly *above* the central laser frequency (see Fig. 1). In fact the $^1F_3$ level lies below the full 5s*n*f $^1F_3$ $n\geq 4$ Rydberg series and has both 4d5p (~25-30%) and 5s*n*f character [50]. Similarly, the 5s7p $^1P_1$ state also comprises about 13% of doubly excited 4d5p character [48,50]. Passing now to the four-photon level, we find that the available 5s$\varepsilon\ell$ continua with ℓ=J=0, 2 and 4 are mixed by CI with a number of near-resonant autoionizing states. Specifically, the effective laser bandwidth comprises the whole 4d5d doubly excited configuration [48] and notably the $^1D_2$ level shown in Fig. 1. The J=0, 2 states are additionally expected to have an important admixture of $5p^2$ character [51]. As for the range above the 4d threshold (vicinity of the fifth photon), it is dominated by the spectrally broad low-lying members of $[5pns]_{J=1}$ [52] and $[5pnd]_{J=1,3}$ [53] series. Lastly, no doubly excited states are expected in the vicinity of the sixth photon, while the seventh and higher photon ranges are largely unexplored and the data are fragmentary [54].

Having the above presentation in mind one may anticipate that the aforementioned configuration mixings may trigger excitation ladders connecting doubly excited states at each step. As an example, consider the process,

$$\left|5s^2\right\rangle \xrightarrow{+3\omega} \left|...+4d5p\right\rangle \xrightarrow{+\omega} \left|...+4d5d+5p^2\right\rangle \xrightarrow{+\omega} \left|5p_j ns\right\rangle \xrightarrow{+\omega} \left|5p_j \varepsilon p\right\rangle, \quad (10)$$

which is also depicted schematically in Fig. 2 and which describes a possible $5p_j(0)$ ionization pathway producing Sr^+ excited to its $5p_j$ state. Although in this example each ladder step was chosen to mainly involve single electron transitions, overall both valence electrons are excited. Therefore, ladders of this type cannot be formed in the absence of electron-electron correlation and level structure embedded in the continuum, this situation being a specific feature of alkaline earth elements. As a reminiscent of these facts the relevant ionization pathways are hereafter labeled as CI-ATI. Nevertheless, typical ATI is also possible here, leaving the ion always in the same excited state [4]. Thus, the $5p_j(1)$ pathway in Fig. 1 involves both CI-ATI and ATI. In general, these two processes may run in parallel, each delivering a quite specific PES that constitutes its fingerprint.

Finally, in order to discuss double ionization we need to emphasize that the reference to electron correlation notions made here differs qualitatively from the one invoked for the description of non-sequential double electron ejection under the influence of strong, short-pulse and long wavelength laser fields [37-39]. In the latter case “correlation” refers to collisional effects between two “quasi-free” electrons that are induced by the interacting laser field. By contrast, the presently discussed CI-ATI relies on the atom-specific bound and autoionizing energy level structure, although this structure can, up to a certain extent, be perturbed by the laser field. Moreover, while CI-ATI may also lead to non-sequential (or “direct” [5]) double ionization, all the processes described by Eqs. (3)-(9) lead to sequential multiphoton double ionization. We denote double ion

production out of a given initial ionic level as $Sr^{2+}(n_i\ell_i,k)$ and Fig. 1 shows the examples of the following $Sr^{2+}(5s,k)$ and $Sr^{2+}(5p_j,k)$ pathways,

$$Sr^{2+}(5s,k): \quad Sr^{+}(5s) + (8+k)\omega \rightarrow Sr^{2+} + e\ (1.37\ eV + k\omega) \tag{11}$$

$$Sr^{2+}(5p_j,k): \quad Sr^{+}(5p_j) + (6+k)\omega \rightarrow Sr^{2+} + e\ (1.21\ eV(j=3/2)/1.31\ eV(j=1/2) + k\omega). \tag{12}$$

Like Eqs. (3)-(9), we include here the possibility of ATI, while the reported k=0 electron energies apply in the absence of ponderomotive or AC Stark shifts and Freeman resonances.

IV. RESULTS AND DISCUSSION

A. Sr^+ and Sr^{2+} yields

The Sr^+ and Sr^{2+} ion yields as a function of laser intensity are presented in Fig. 3. We note first that below saturation the singly charged ion yield follows an I^{K_+} power-law with an apparent slope of $K_+ \approx 4$. Saturation occurs at ~6 TWcm^{-2} i.e. at a value which is higher than the one reported earlier for ionization studies via long (~ns) pulses of similar wavelength and processes of the same minimum nonlinearity of ionization [10]. This is to be expected since in the present work pulses of shorter duration (fs) are employed. As for the Sr^{2+} yield, it does not saturate up to the highest intensity of the graph, it exhibits an ionization order of non-linearity of $K_{2+}\approx 3$ and it appears to be detectable at intensities equal to or greater than the above Sr^+ saturation intensity. This is a signature of a sequential double ionization mechanism. It additionally suggests that for I<~5 TWcm^{-2} we can ignore, to a first approximation, double ionization processes for the analysis of the PES.

Although not related to our main focus on the study of CI-ATI processes, it would be interesting at this point to open a parenthesis and briefly discuss the connection of the presently recorded data with the aforementioned alkali atom ionization studies. In order to implicate over-the-barrier concepts to this discussion, let us first use the most frequently employed 1D expression for the critical intensity I_{OBI} which writes (in atomic units) [15,20],

$$I_{OBI} = \left[\frac{\kappa^4}{16 Z_{eff}}\right]^2 \tag{13}$$

where Z_{eff} is the effective charge of the residual ion and $\kappa = \sqrt{2IP}$ (atomic units). It is presently accepted that this expression underestimates I_{OBI} [15]. Indeed, for Sr atom (IP=5.7 eV, Z_{eff}=1) Eq. (13) predicts I_{OBI}(Sr)≈4 TWcm^{-2}, which is close to the values reported for several alkali atoms with comparable IPs [19,22,25]. However, it lies below the saturation intensity of the Sr^+ yield, contrary to the expectation that for $I \geq I_{OBI}$ the ionization probability should be unity (saturated ionization process) [25]. Similarly, for Sr^+ (IP=11.03 eV, Z_{eff}=2) Eq. (13) predicts $I_{OBI}(Sr^+)$≈15 TWcm^{-2}, again

far below saturation. A presumably more accurate estimate for I_{OBI} may be obtained by adopting the less familiar 3D formula based on the parabolic coordinates (ξ,η,φ) [20,55] (in atomic units),

$$I_{\mathrm{OBI},\eta} = \left[\frac{\kappa^4}{16Z_{eff} - 8\kappa}\right]^2 \tag{14}$$

where the symbol $I_{\mathrm{OBI},\eta}$ is used for making the distinction from Eq. (13). Yet, both estimates rely on the static field concept. Using Eq. (14) we find $I_{\mathrm{OBI},\eta}(\mathrm{Sr})\approx 9$ TWcm^{-2} and $I_{\mathrm{OBI},\eta}(\mathrm{Sr}^+)\approx 25$ TWcm^{-2}, which appear more compatible with the yields of Fig. 3 despite the $\gamma>1$ condition holding over the whole intensity range of the present experiment (see upper x-axes of Fig. 3) and suggesting an MPI picture. A finer characterization of the ionization regime is to be provided by the following analysis of PES.

B. Evolution of PES with laser intensity

Typical PES recorded within the $4\leq\gamma_{\mathrm{Sr}}\leq 1.2$ and $5.5\leq\gamma_{\mathrm{Sr}^+}\leq 1.7$ intervals are given in Figs. 4 and 5. Figure 4 presents a collection of the data corresponding to the higher intensity interval (roughly 7-24 TWcm^{-2}) where the singly charged Sr^+ ion is saturated and double ionization is efficient ($\gamma_{\mathrm{Sr}}<2.8$ and $\gamma_{\mathrm{Sr}^+}<3.9$). Within this interval the PES evolve from typical single-active-electron ATI structures towards a mixed ATI-tunneling regime. In the following presentation the ATI series are discussed first because they will serve as a "reference" when seeking points of departure from their apparently simple structure. The points of departure from this reference at higher intensities concern the above mentioned onset of tunneling which is discussed afterwards. Although a byproduct of the present study with no connection to CI-ATI signatures, this mixed regime is here commented for completeness and for making again a connection with earlier recent research devoted to strong field nonlinear ionization of the alkali atoms. As for the finally discussed points of departure from the typical ATI structures that are related to CI-ATI, i.e. to the main subject of interest in the present work, they are evident in the PES given in Fig. 5. This graph shows typical spectra concerning the lower intensity interval, 3.7-5 TWcm^{-2}, where the Sr^+ yield is unsaturated and Sr^{2+} appears to be undetectable. Below we analyze the spectra of these two graphs in more detail and invoke the relevant PADs when necessary, for shedding light on the involved ionization mechanisms.

1. Intensity range above the Sr^+ saturation intensity: ATI structures

We focus first on the "reference" curves 4(a) and 4(b) whose main feature is the presence of several strong ATI peaks. The curve of Fig. 4(a) is recorded at $I \approx 6.7$ TWcm^{-2}, where the Sr^{2+} signal is apparent. Therefore, it is reasonable to assume that the observed ATI series stem from both single and double ionization processes (the latter contributing a much weaker signal to the total one). A careful look on the lower energy and strongest ATI members reveals a double peak structure that implies the simultaneous presence of two ATI series. Actually, two members of a third quite weak ATI series are also visible in the spectrum of Fig. 4(a) and the corresponding inverted VMI image given in its inset. Note further that within the examined intensity range the peaks of all three series remain practically unshifted with varying intensity. This peak stabilization cannot stem from a cancellation effect between U_p and initial state AC Stark shifts. For the atomic system this is ruled out because the low energy ATI peaks do shift at lower intensities. By using theoretical values of dynamic dipole polarizabilities and corresponding AC Stark shifts [56] we verified that the ionic system suffers no such type of cancellation as well. In another scenario, since the Sr^{+} yield is saturated, ionization could occur at the same intensity which is reached at the leading edge of the pulse and irrespective of its maximum value [19,20,25]. Nevertheless, this scenario is improbable for the spectra of Figs. 4(a,b) because within this intensity range the ATI structure continues to develop and the number of ATI peaks increases with I. Furthermore, this scenario is irrelevant for the ionic system (unsaturated Sr^{2+} signal). Consequently, the effect has to be attributed to the presence of Freeman resonances whose energy location is indeed approximately independent of I.

Dealing with the atomic system first, we find that there is only one singlet three-photon Freeman resonance due to the bound 5s6p $^1P_1$ state (see Fig. 1) that is compatible with the spectrum of Fig. 4(a) at the given laser intensity. The latter is very close to the $I_{thr} \approx 7.2$ TWcm^{-2} threshold intensity of appearance for this resonance, as estimated by setting $\Delta E_{5s^2}=0$ and using the equation $[E_{5s6p\ ^1P_1} + U_p(I_{thr})]=3\omega$. In fact, since experimentally this peak stabilizes at $I \approx 6$ TWcm^{-2}, it is reasonable to assume that the actual threshold is somewhat lower than the above value (as implied by the condition $\Delta E_{5s^2}<0$ – see the calculation of Refs. [57]). Furthermore, this resonance is expected to produce ≈0.08 eV electrons, i.e. approximately equal to the energy of ~0.1 eV corresponding to the *non-resonant* 5s(k=0) process. These numbers are compatible with the ~0.2 eV experimental location of this peak, particularly if our spectrometer's resolution and laser bandwidth are taken into account. Additionally, the corresponding angular distribution (see inset of Fig. 4(a)) reveals a pronounced d-wave contribution, implying a 5s6p → 5sεd ionization step at the four photon level. Remarkably, the presence of the ~0.2 eV peak persists well above the channel-closing intensity for the non-resonant 5s(0) process (≈8.6 TWcm^{-2}, as predicted by Eq. (1) for $\Delta E_{5s^2}=0$). Its persistence may be attributed to the spatio-temporal intensity distribution of the laser beam and particularly to a laser-atom interaction volume effect [21]. Specifically, it may be attributed to the existence of a

"slice" of this volume where the intensity ranges between the resonance threshold and the 5s(0) channel-closing intensities, despite the much higher values the peak intensity may acquire at the laser beam center. Furthermore, the fraction of this slice over the total volume gets smaller with rising intensity, a fact that is reflected in the gradually decreasing magnitude of this peak. On the other hand, even under these conditions Fig. 4(b) (where I = 14 TWcm^{-2}) reveals the clear presence of the k=9 member of the ≈0.2 + $k\omega$ eV (k≥0) *resonant* atomic ATI series, implying that the energy absorbed by the single-active-electron largely exceeds the double ionization limit of Sr.

The two remaining ATI series should stem from the ionic system. Recall first that the atomic ATI process presented above leads to the production of ground state Sr^+ ions. Additionally, within this intensity range the data show no evidence of excited ionic state populations. Hence, the 5s ionic ground state is expected to be the only initial state available for double ionization. This is largely confirmed by the fact that the members of the stronger ionic ATI series (appearing as weak shoulders on the strong atomic ATI peaks) best fit the Sr^{2+}(5s,k≥0) process, observed at ≈1.36 + $k\omega$ eV, i.e. very close to the predictions of Eq. (11). They do not shift with intensity, pointing again towards the existence of Freeman resonances. By inspecting the energy levels diagram of the ion [47] one indeed finds an appreciable number of closely-spaced, seven-photon resonant nf Rydberg states of Sr^+ (see Fig. 1), where the 1.36 eV energy of the k=0 peak corresponds to n≈17. The relevant threshold intensities of appearance are very low and these Freeman resonances can come into play as soon as MPI of ground state ions is feasible. In fact, the situation is even more complicated by the additional presence of the quasi-resonant 7d state in the vicinity of the sixth photon. Without taking into account any AC Stark shifts this resonance would produce ≈1.32 eV electrons. However, an accurate estimation of the AC Stark shift due to this double (or even multiple) resonant 7d-nf effect should probably necessitate non-perturbative theoretical calculations [7,58,59]. Thus, the behavior of the 7d state is difficult to predict but we may speculate that it could lead to another Freeman resonance and the creation of an electron peak at a different and largely displaced location with respect to the one at 1.36 eV. In fact, this is a possible origin of the third quite weak ionic ATI series at ≈0.78 + $k\omega$ eV (k=0,1) observed noticeably in Fig. 4(a), for which there is no other obvious scenario involving the Sr^+ ground state.

2. Intensity range above the Sr^+ saturation intensity: Onset of tunneling ionization

A typical PES near the highest available intensity is given in Fig. 4(c). We may observe that as I increases the higher members of all aforementioned ATI series are practically washed-out in favor of a considerable background. The few remaining lower energy ATI members broaden and their contrast relative to the background decreases with increasing intensity. In fact, the background

starts to develop progressively from lower intensities and it is already quite apparent in Fig. 4(b). Its origin, along with the disappearance of the ATI structure, is typically associated with the departure from the MPI picture and the gradual dominance of the tunneling and over-the-barrier ones [15,60]. It is highly probable that the simultaneous presence of ATI and tunneling (and/or over-the-barrier) signatures is to be attributed to the spatio-temporal intensity distribution of the laser beam. It is interesting to note, however, that in our case a large fraction of Sr atoms and/or Sr^+ ions seem to actually survive ionization until the maximum laser pulse intensity is reached. On the other hand, the data of Fig. 4(c) were recorded at $I>I_{OBI,\eta}(Sr)$ and $I\approx I_{OBI,\eta}(Sr^+)$, while $\gamma>1$, a situation reminiscent of strong-field nonlinear ionization of the alkali atoms. In an attempt to resolve this apparent conflict, we adopt the nowadays widely accepted view that the Keldysh parameter alone is not a sufficient indicator for characterizing the ionization regime. Quite frequently, two additional dimensionless indicators are also introduced, namely $z=2/\gamma^2$ and $z_1 = U_p/\omega$ [61,62]. Then, "pure" MPI necessitates $\gamma>1$ *and simultaneously* $z<1$ and $z_1<1$ [62]. In the opposite case ($\gamma<1$ *and simultaneously* $z>1$ and $z_1>1$) tunneling or even over-the-barrier ionization prevails. Accordingly, the regime where $\gamma>1$ but either one of z or z_1 or both of them are larger than unity may be termed as the "intermediate regime", implying a certain mixture between MPI and tunneling conditions. In our case, starting with z_1 which is independent of the target system and characterizes solely the laser field, we find that it becomes larger than unity for $I \geq 26$ TWcm^{-2}, this value being very close to our highest available intensities. Furthermore, one finds $z(Sr)\geq 1$ for the comparable lower bound $I\geq 24$ TWcm^{-2}, while the condition $z(Sr^+)\geq 1$ is fulfilled for higher intensities outside the range of the experiment. Evidently, these estimates are fully coherent with respect to the experimental data and point with enough certainty towards the "intermediate regime". In fact, this is true for both the atom and the ion (due to z_1 and because Sr^+ is "fed" by the neutral atom ionization). The above discussion closes our parenthesis on the mixed MPI-tunneling ionization conditions.

3. Intensity range below the Sr^+ saturation intensity: CI-ATI signatures

We now turn to the data of Fig. 5 concerning the 3.7-5 TWcm^{-2} intensity range and characterized by the presence of CI-ATI processes. The figure also includes a "reference" PES recorded at $I \approx 5$ TWcm^{-2}. This latter PES exhibits all the ATI structures discussed above, the difference with respect to the higher intensity data of Fig. 4 being that most ATI peaks appear now to red-shift with increasing intensity. Thus, they reflect primarily the non-resonant 5s(k) and Sr^{2+}(5s,k) processes and they are not yet fully dominated by Freeman resonances. The predictions of Eq. (1) with $\Delta E_{5s^2}=0$ are superimposed on the spectrum and reproduce well the locations of the 5s(1) and 5s(2) peaks, but only approximately the location of the 5s(0) one. Using the calculated

value for ΔE_{5s^2} [57] the agreement worsens for all three peaks. We may conclude that in our case atomic AC Stark shifts are generally far more complicated than that implied by Eq. (1) [59]. Therefore, we set $\Delta E_{5s^2}=0$ in the following and assume that the predictions of Eq. (1), although quite useful, indicative and informative, are quantitatively somewhat inaccurate.

Interestingly, the spectra of Fig. 5 probe weak double ionization processes within the $4.3 \leq I \leq 5$ TWcm^{-2} intensity range where no Sr^{2+} signal appears in the log-log plot of Fig. 3. This is not fully understood. A possible explanation could involve spatial non-uniformities in the detection efficiency of the MCPs for electrons and ions. Whatever the reason, however, this observation suggests the assumption that no double ionization occurs below the saturation intensity of the Sr^+ yield should be taken with caution in the following analysis, where, perhaps, a possible weak Sr^{2+} production (<5% of the total ion signal as visible on Fig. 3) could be taken into account.

Finally, in order to compare with the lower intensity data, it is interesting to inspect the $I \approx 5$ TWcm^{-2} "reference" PADs given in Fig. 6 for the strong 5s(k) ATI peaks. The PAD of the 5s(0) peak at ≈0.3 eV is to be compared with the one seen in the inset of Fig. 4(a). They both clearly point towards a dominant contribution from the 5sεd continuum (note the strong signal perpendicularly to the laser polarization direction, i.e. at θ=90^o). The $I \approx 5$ TWcm^{-2} 5s(0) PAD additionally exhibits a weak side lobe within the $0^o<\theta<90^o$ interval, probing a quite small 5sεg contribution. These PAD shapes are similar to the ones reported earlier for four-photon ionization via long (~ns) pulses, for either Mg [9] or Sr [12] out of their respective ground states. Based on them one can easily understand the quite asymmetric shape of the 5s(1) PAD at ~1.9 eV which, as Fig. 6 shows, is characterized by a quasi-zero signal at $\theta = 90^o$ and an intense side lobe within $0^o<\theta<90^o$, revealing a dominant 5sε'f contribution. As for the 5s(2) PAD, it is not shown in Fig. 6 but it is identical to the one observed in the inset of Fig. 4(a) and displays a reappearing θ=90^o local maximum and a dominant 5sε''g contribution.

Having presented above all the required reference information, consider next the lower intensity PES of Fig. 5 which reveal a richer and somewhat more complicated structure with respect to their highest intensity counterparts. This is also qualitatively evident from the inverted images of Fig. 6. Let us begin the analysis of this different structure by the <0.2 eV electron peak which, as laser intensity increases, gradually shifts towards lower energy, weakens in magnitude and disappears. From Eqs. (1) and (3)-(9) we expect contributions to this signal from the 4d(0) and 7s(0) processes. Nevertheless, one may reasonably expect the 4d(0) ionization pathway to be the by far dominant one due to its much lower number of photons involved (i.e. the much lower nonlinearity of ionization) and the somewhat higher energy of the released electron. The disappearance of this peak is attributed to the closing of this channel ($\varepsilon_{4d,5}=0$) and occurs at ≈4.8 TWcm^{-2} (for $\Delta E_{5s^2}=0$ Eq. (1) predicts a somewhat lower disappearance intensity of ~4 TWcm^{-2}). More importantly, its

presence ensures the emergence of population in the 4d ionic state, thus signaling the presence of CI-ATI processes. On the other hand, it is verified that double ionization out of this ionic level does not occur since the relevant electron peaks are absent. Finally, the low intensity spectra of Fig. 5 suggest the weak presence of the 4d(1) peak at ≈1.5 eV, most probably blended with peaks corresponding to other processes discussed below.

Let us deal next with the strongest in magnitude and fairly complex structure observed in the PES of Fig. 5 within the 0.2 - 0.7 eV interval. For low laser intensity this structure consists of three distinct but partially overlapping lines. As intensity grows it gradually evolves to a single peak clearly attributed to the 5s(0) process. The predictions of Eq. (1) for $\Delta E_{5s^2}=0$ drawn in Fig. 5 help us identify the possible candidates for these three peaks at $I \approx 3.7$ TWcm^{-2}. These are the 5s(0) one, the two $5p_j(0)$ spin-orbit components and, finally, the 6s(0) and 4f(0) ones (the latter two being practically indistinguishable at this energy scale). Among the pathways leading to excited ion formation, the presence of the $5p_j(0)$ one appears to be the most probable one, due to its much lower nonlinearity of ionization. In fact, since all three peaks are separated by an energy difference of ≈0.1 eV which matches the ionic 5p level spin-orbit splitting, it is possible that two out of the three peaks belong to the $5p_{1/2,3/2}(0)$ components. The third peak of the triplet could just be the 5s(0) one. However, none of the three corresponding PADs of Fig. 6 at I≈3.7 TWcm^{-2} resembles the one at I≈5 TWcm^{-2} discussed above and they simply cannot be reproduced by a fit including solely the $5s\varepsilon\ell$, ℓ=0,2,4 continua. Instead, they all are fairly complex, having several local extrema between θ=0^o and θ=90^o, they are "symmetric" (approximately equal signals at θ=0^o and θ=90^o) and they seem compatible with decay channels corresponding to excited ionic levels, like the $5p_j\varepsilon\ell$ ones. Therefore, at low intensity no peak of the triplet appears to primarily belong to the 5s(0) process. This fact is a reminiscent of the observations made in earlier Sr ionization studies with long (~ns) and low intensity pulses, same orders of non-linearity and similar wavelength [12], where the excited 4d and 5p ionic levels were found to be by far more populated than the 5s ground state. As for the remaining candidates, namely the 6s(0) and 4f(0) processes, one would expect them to have significantly lower signal than the $5p_j(0)$ one, due to their much higher nonlinearity and the anticipated substantial atomic population decay to electron - Sr^+ pairs at each photon absorbed within the continuum. Consequently, a more clear picture for the 6s(0) and (to a lesser degree) the 4f(0) channels may be achieved only after considering the origin of the remaining electron peaks.

As seen in Fig. 5, the electron energy expected for the $5p_j(1)$ process lies very close and overlaps with the 5s(1) one, particularly if the effective laser bandwidth is taken into account. For distinguishing between the two processes and observing their competition with varying intensity we invoke the PAD at the maximum of the relevant peak located at ≈1.9 eV. The intensity evolution of

this PAD is given in Fig. 6, along with the high intensity "reference" probing the 5s(1) pathway already discussed above. With respect to that PAD, the $I \approx 3.7$ TWcm^{-2} one is completely different and evidently related to the PADs of the triplet structure within the 0.2 - 0.7 eV range for the same intensity. Specifically, this PAD also exhibits several local extrema between θ=0^o and θ=90^o and comparable signals at these two angles. Consequently, this PAD excludes the 5s(1) pathway and, more notably, it probes the 5p$_j$(1) process, because there are no other (single or double ionization) processes expected at this energy. Fig. 6 shows that as intensity increases the 5s(1) and 5p$_j$(1) pathways coexist, resulting to an incoherent sum of two PADs [63] and a θ=90^o signal gradually diminishing and favoring the pure 5s(1) PAD. As a last remark on this spectral feature, we may anticipate that the emergence of a single broad 5p$_j$(1) peak instead of a j=1/2,3/2 doublet is to be most probably attributed to its blend with the peaks of other processes and to the increased effective laser bandwidth.

There is a last remaining quite weak peak to be discussed. It is observed in the low intensity PES of Fig. 5 at ≈1.0 eV and disappears for $I > 4.3$ TWcm^{-2}. Given the proven presence of the 5p$_j$(1) pathway, the energy location and low magnitude of this peak correlates well with the 6p(0) process (and would also support a contribution of the 6s(0) channel related to the ≈0.59 eV peak of the 0.2 - 0.7 eV triplet). However, although unlikely, this peak could also emerge from the Sr^{2+}(5p$_j$,0) double ionization process. If only the ponderomotive shift is included in Eq. (12) we indeed expect a ~1 eV energy peak, while if the calculated AC Stark shift of the 5p$_j$ levels [56] is also included its energy is found to be <<1 eV. Still, a ~1 eV peak may be produced if Freeman resonances are considered for the *resonant* Sr^{2+}(5p$_j$,0) pathway, but such a possibility is rather weak because the observed peak slightly downshifts with increasing intensity. The same reasoning applies also for the double ionization pathway out of the 6s ionic level.

The findings presented above reveal the presence of CI-ATI processes at low intensity. Indeed, the analysis of relevant PES and PADs led to the detection of, at least, the 4d(0) and 5p$_j$(1) CI-ATI pathways (for the former the other less probable candidate is also a CI-ATI process). Moreover, the emergence of channel 5p$_j$(1) (which implies the absorption of three CI-ATI photons) requires the presence of the 5p$_j$(0) one as a prerequisite. For the latter pathway the relevant electron peak appears to be indeed present in the PES, but it is blended with other peaks within the 0.2 - 0.7 eV range. This blend renders the detailed assignment of theses peaks rather incomplete and difficult to achieve at present. Nevertheless, it is to be emphasized that our study does not mainly focus on their identification. Instead, it focuses on the proved observation of CI-mediated absorption processes, as well as on the transition towards the single-active-electron behavior as intensity increases. These facts are very clearly registered in Figs. 5 and 6. It is finally important to note that the proof of CI-ATI presence is here based solely on experimental data and without any prior or

complementary reference to theoretical calculations. On the other hand, theoretical modeling would be, of course, highly desirable for providing further insight.

V. CONCLUDING REMARKS AND FUTURE PERSPECTIVES

We have presented measurements of a photoelectron spectroscopy study devoted to the nonlinear single and double ionization of Sr atoms interacting with ≈800 nm laser pulses of ≈25 fs duration. Within the examined laser intensity range, photoelectron energy spectra and angular distributions probe two consecutive transitions between processes of qualitatively different nature. At low intensity, $I \leq 4$ TWcm^{-2}, the recorded data revealed the production of excited singly-charged ions, thus proving that single ionization proceeds via excitation ladders composed by quasi-resonant doubly excited states. The emergence of dense manifolds of the latter states just above (or even below) the first ionization threshold characterizes Sr and the other alkaline earth atoms and it has been the point of focus in the present work because of the strong interaction between the two valence electrons it implies. However, this mechanism is rather abruptly turned-off at higher intensity where it is replaced by a single-active-electron one which is probed by the observation of typical atomic and ionic ATI structures. Finally, by increasing the intensity even further the MPI picture gradually diminishes in favor of tunneling ionization.

We have shown that this last MPI-to-tunneling ionization transition, while unexpected on the basis of the Keldysh parameter alone, can be explained by additionally implicating several other indicators for properly characterizing the ionization regime. These indicators provided an estimated intensity of ≈24 TWcm^{-2} that separates the two regimes and this value roughly agrees with experimental observations. On the contrary, there is no clear explanation concerning the origin of the sharp switching-off of the electron correlation mediated processes. In the relevant earlier work devoted to Mg atom [32], the results of a rate equation model attributed this switching-off to the small population accumulated to the excited ionic state as compared to the ground state of Mg^+, as well as to the fast depletion of this excited population with increasing intensity. This does not seem to be the case in the present experiment, where excited ionic state populations appear to be considerably larger than the ionic ground state one at low intensity. Thus, an alternative explanation is required. In the absence of any theoretical results stemming from an appropriate model including two electron effects, we tentatively attribute the effect to the blue shift of the 4d5p $^1F_3$ and 5s7p $^1P_1$ three-photon near-resonant states with increasing intensity. These states exhibit considerable mixing among doubly excited and singly excited (Rydberg) configurations and constitute the first ladder step. Thus, their blue shift (either the ponderomotive or a more subtle AC Stark one) would push them out of resonance, destroying this way the whole ladder structure. In addition, the 4d(0)

channel-closing that occurs within the same intensity range may also create unfavorable CI-ATI conditions.

Interestingly, both of the above assumptions can be experimentally put to test, since they can be both remedied, in principle, by increasing the photon energy. An obvious solution would be to repeat the earlier experiments in Sr performed at ≈725±10 nm [12], by replacing the long (~ns) pulses with ultrashort (~fs) ones. These wavelengths can be easily obtained nowadays by optical parametric amplifier systems. This choice, however, presents several shortcomings. First, there is a considerable overlap between the electron energies produced by different pathways. Second, the aforementioned resonances are expected to resonantly upshift at rather high intensities, the latter largely exceeding the Sr^+ yield saturation intensity which is expected to be close to the presently observed one. Therefore, the radiation wavelength needs to be more judiciously chosen. Assuming only the presence of U_p, we estimate that an interesting choice would be to employ ≈740-745 nm radiation. The latter range ensures the 4d(0) channel closing would correspond to an intensity of ~10 $TWcm^{-2}$, which is much higher than the one witnessed at the present experiment and close to the saturation intensity of Sr^+. More importantly, at about the same intensity the upshifted aforementioned states would now be brought into three-photon resonance. Finally, most ionization pathways are expected to produce fairly well resolved electron peaks.

The aim of the above proposals is to push the observation of CI-ATI processes at intensities of the order of 10 $TWcm^{-2}$ or higher. Under such conditions we may even envision an increasing probability to additionally observe CI-mediated direct (or non-sequential) double ionization within the MPI regime. If successful, such experiments would allow bridging with observations of non-sequential double ion production within the tunneling regime [34,37-39]. In this respect, it is evident that the presence of sequential double ionization processes would play an obscuring role. Consequently, the employment of coincidence studies [64] at some stage of this research direction would be unavoidable. Furthermore, it would be highly desirable for the choice of the relevant experimental parameter space to be guided by two-active-electron theoretical modeling (see, for example, Refs. [65,66]). Therefore, recognizing that present day experimental and (to some extent) theoretical techniques have reached a certain degree of maturity, we hope that the work presented here may initiate a different, albeit promising, pathway towards the study of electron-correlation effects in the ultrafast regime.

FIGURE CAPTIONS

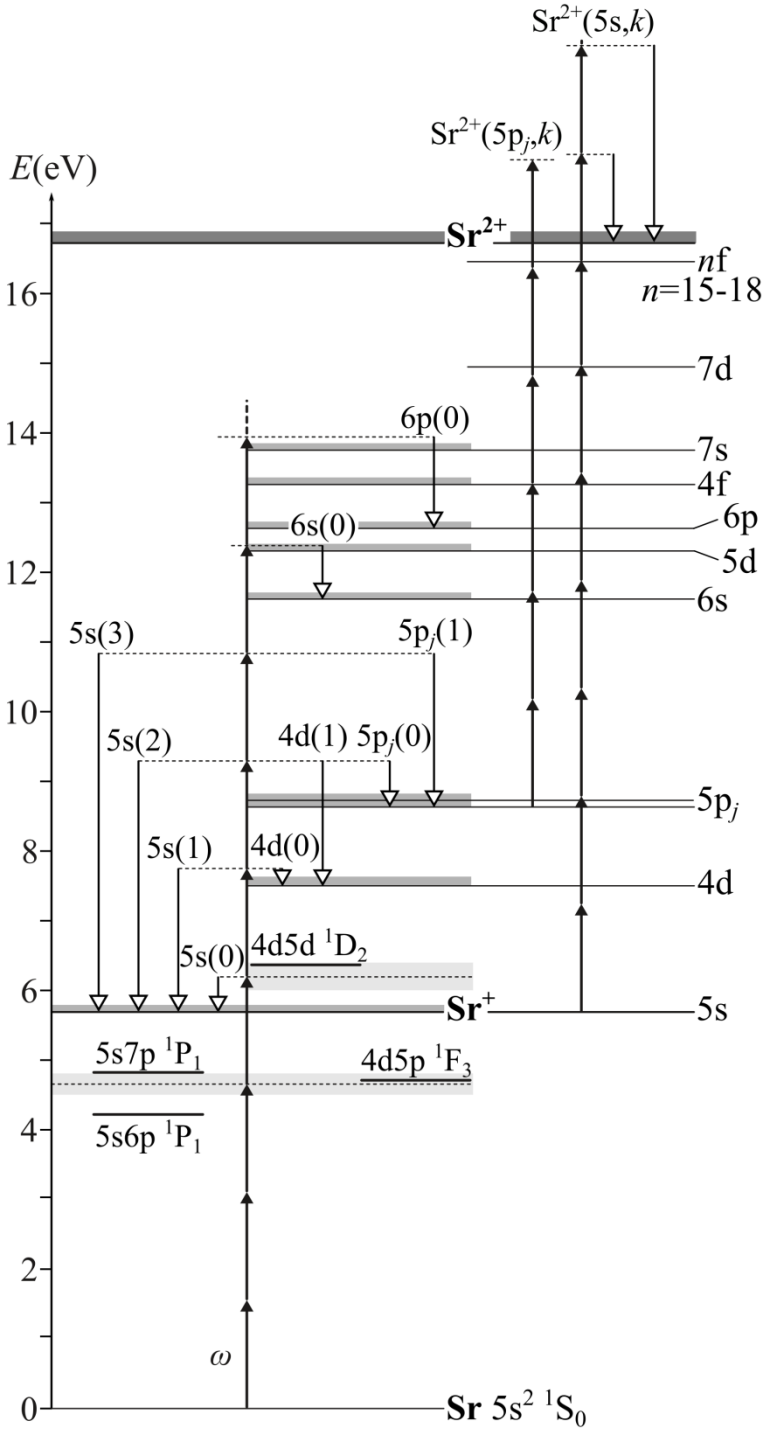

Fig. 1. Partial, in scale, energy level diagram of Sr, depicting the most relevant atomic and ionic levels as well as the possible multiphoton single and double ionization pathways. Dark gray shadings denote the ionization threshold and continua associated with each ionic level and the double ionization limit. Light gray shading denotes the three- and four-photon effective laser bandwidth [49]. For the labeling of ionization processes see the text (and Eqs. (3)-(9)).

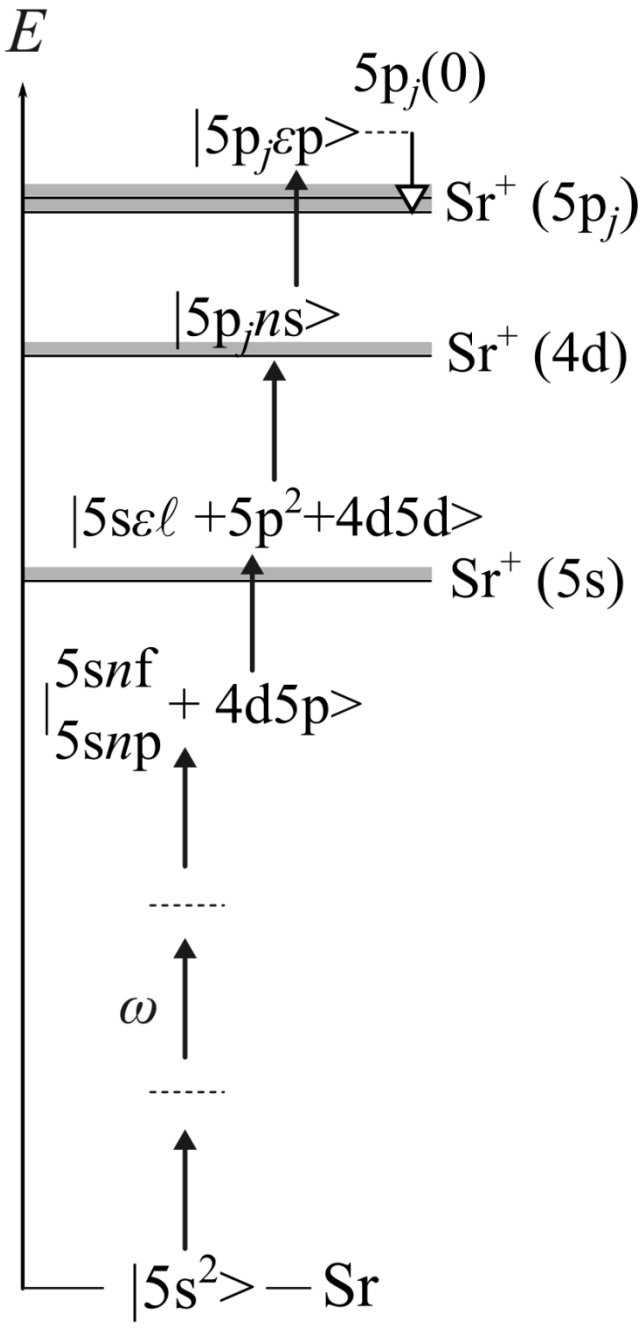

Fig. 2. Schematic diagram of a ladder excitation scheme describing a possible (out of several) $5p_j(0)$ ionization pathway producing excited ions (Eq. (5)). Gray shading denotes the ionization thresholds and continua associated with 5s, 4d and $5p_j$ ionic levels. At this particular scheme each ladder step involves single electron transitions but, overall, both valence electrons are excited. Such ladders necessitate the existence of electron-electron correlation leading to strong configuration interaction and level structure embedded in the continuum, the latter characterizing Sr and the other alkaline earth atoms. Note that the experiment probes the population created in the excited ionic state but not the exact ladder scheme.

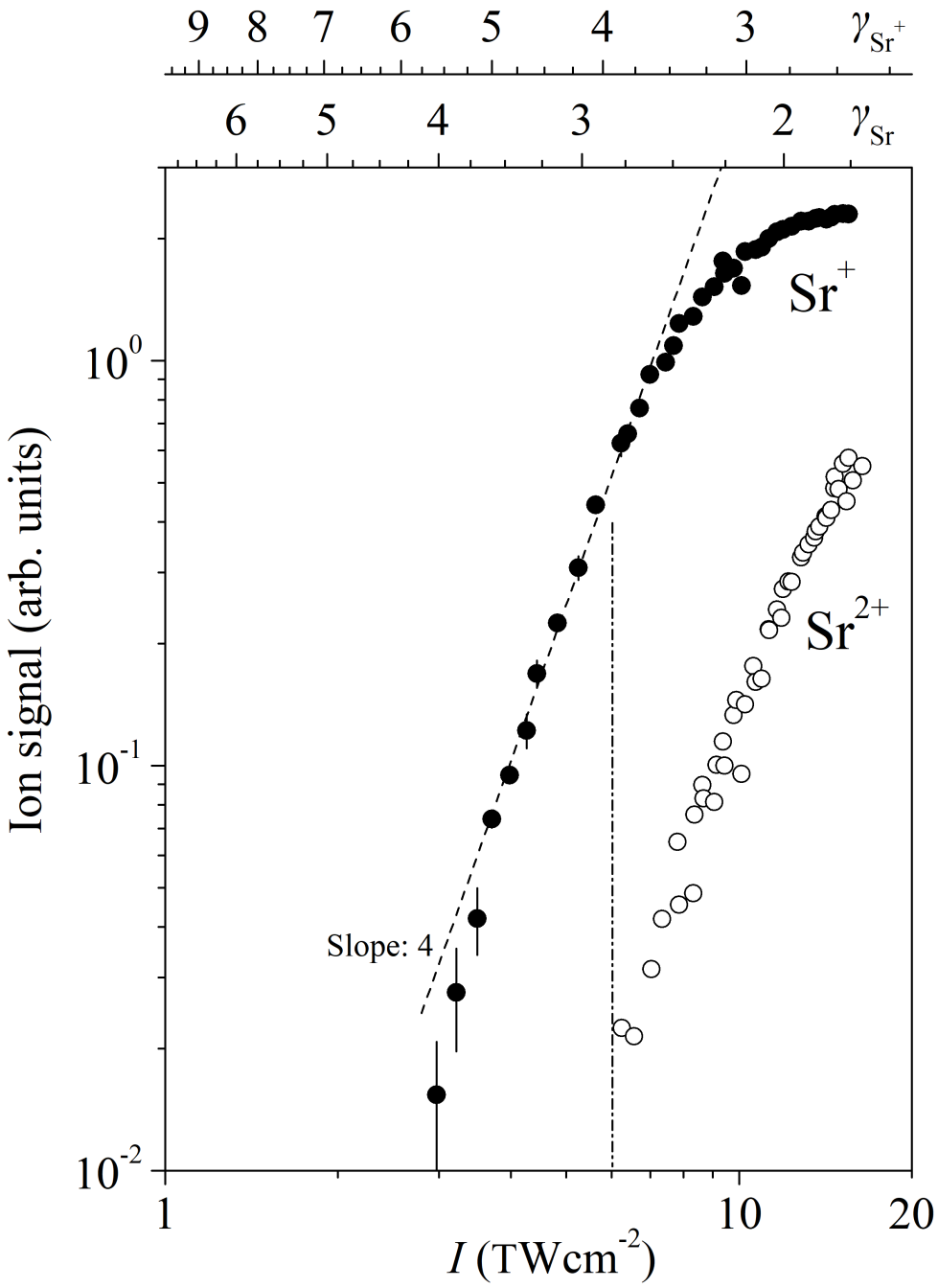

Fig. 3. Log-Log plots of the measured singly and doubly charged Sr yields as a function of laser intensity (lower x-axis) and as a function of the atomic and ionic Keldysh parameters γ_{Sr} and γ_{Sr^+}, respectively (upper x-axes). Whenever the y-axis uncertainties are not indicated they are of the order of the symbol size. A dashed straight line corresponding to an I^4 intensity dependence is matched to the unsaturated part of the Sr^+ curve. The latter is separated from the saturated one by the vertical dashed-dotted line. A quantifiable Sr^{2+} signal appears for intensities above the Sr^+ saturation intensity. A fit of the doubly charged ion signal as a function of I yields an $I^{3.0\pm0.1}$ intensity dependence (not shown).

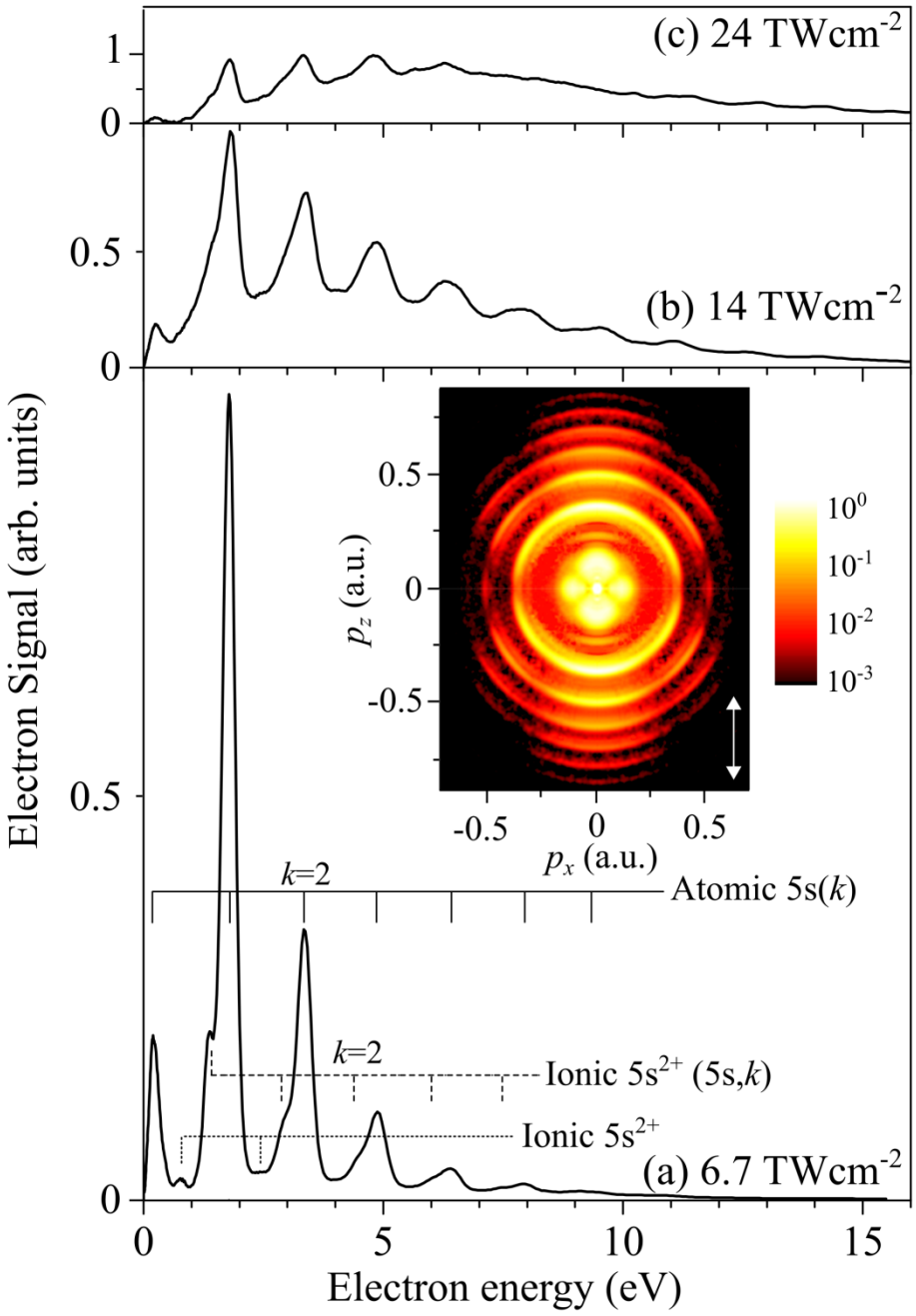

Fig. 4. Electron energy spectra acquired at the laser intensity values specified at each plot. The maximum signal of each PES is set equal to unity. In (a) the members of the atomic and ionic ATI series discussed in the text are indicated. The corresponding inverted (and symmetrized) image given in the inset shows the photoelectron momentum distributions (in atomic units - a.u.)/PADs. For better visibility of its weak features the image is drawn in logarithmic color scale covering three orders of magnitude (see the given color bar). The white double-headed arrow shows the direction of the linear laser polarization. Note that in (b) the number of ATI members increases further and a background starts to build up, while this background dominates in (c) and the ATI structure is greatly washed-out.

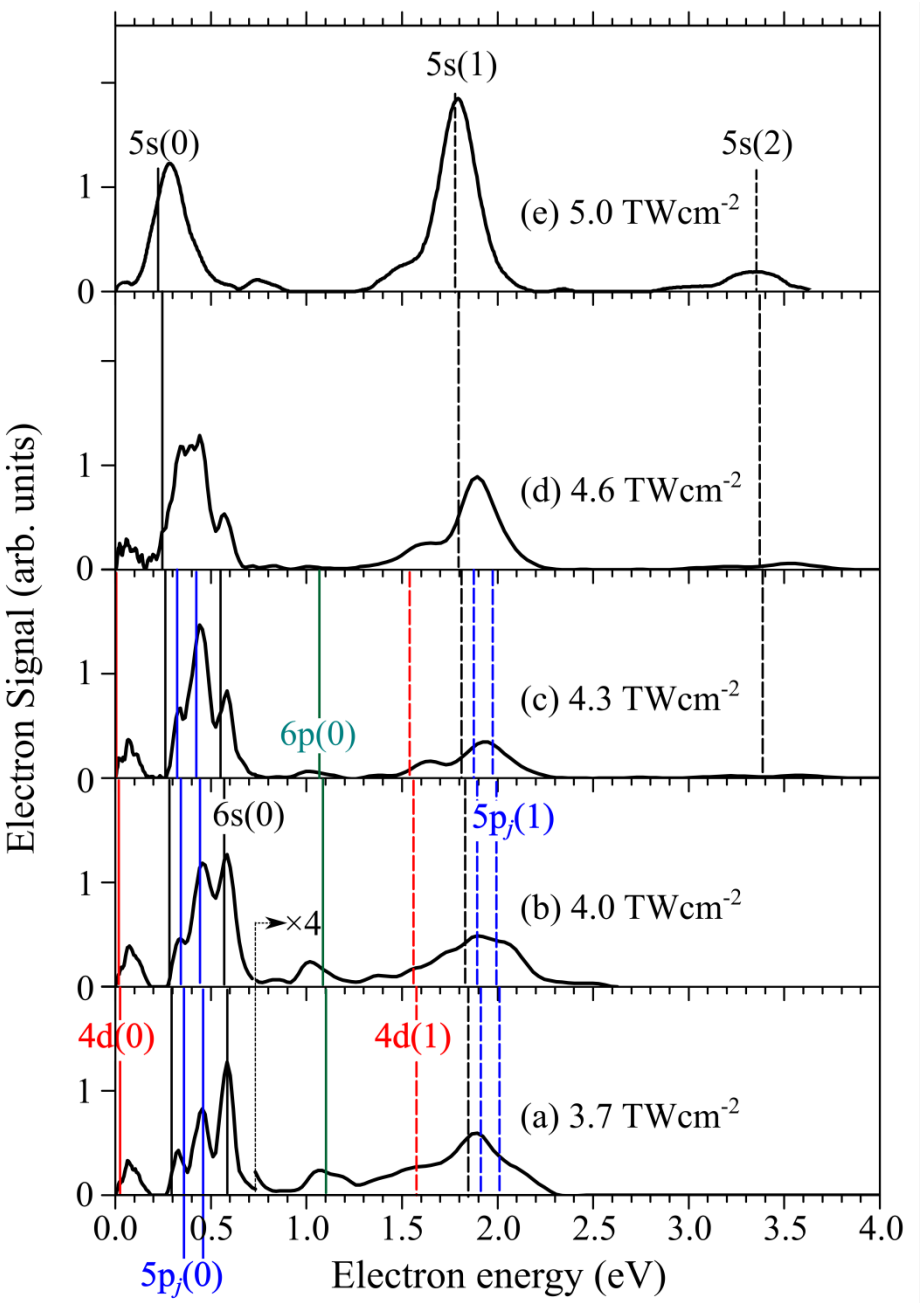

Fig. 5. Electron energy spectra acquired at the lower intensity range 3.7-5 TWcm^{-2}. The location of each spectrum along the y-direction is proportional to the intensity of the particular recording which is specified at each plot. For facilitating the discussion given in the text the graph also includes the predictions of Eq. (1) for the single ionization pathways of Eqs. (3)-(7), (k=0 full vertical lines, k>0 dashed vertical lines) after including only the ponderomotive shift U_p. The 5s^2 ground state AC Stark shift is ignored (i.e. ΔE_{5s^2}=0) because its inclusion using the existing theoretical value [57] considerably worsens the agreement with all experimental data. Furthermore, since within this intensity range double ionization is not apparent in Fig. (3), the relevant ionization processes are not included in the graph (for a more detailed discussion of this point see text).

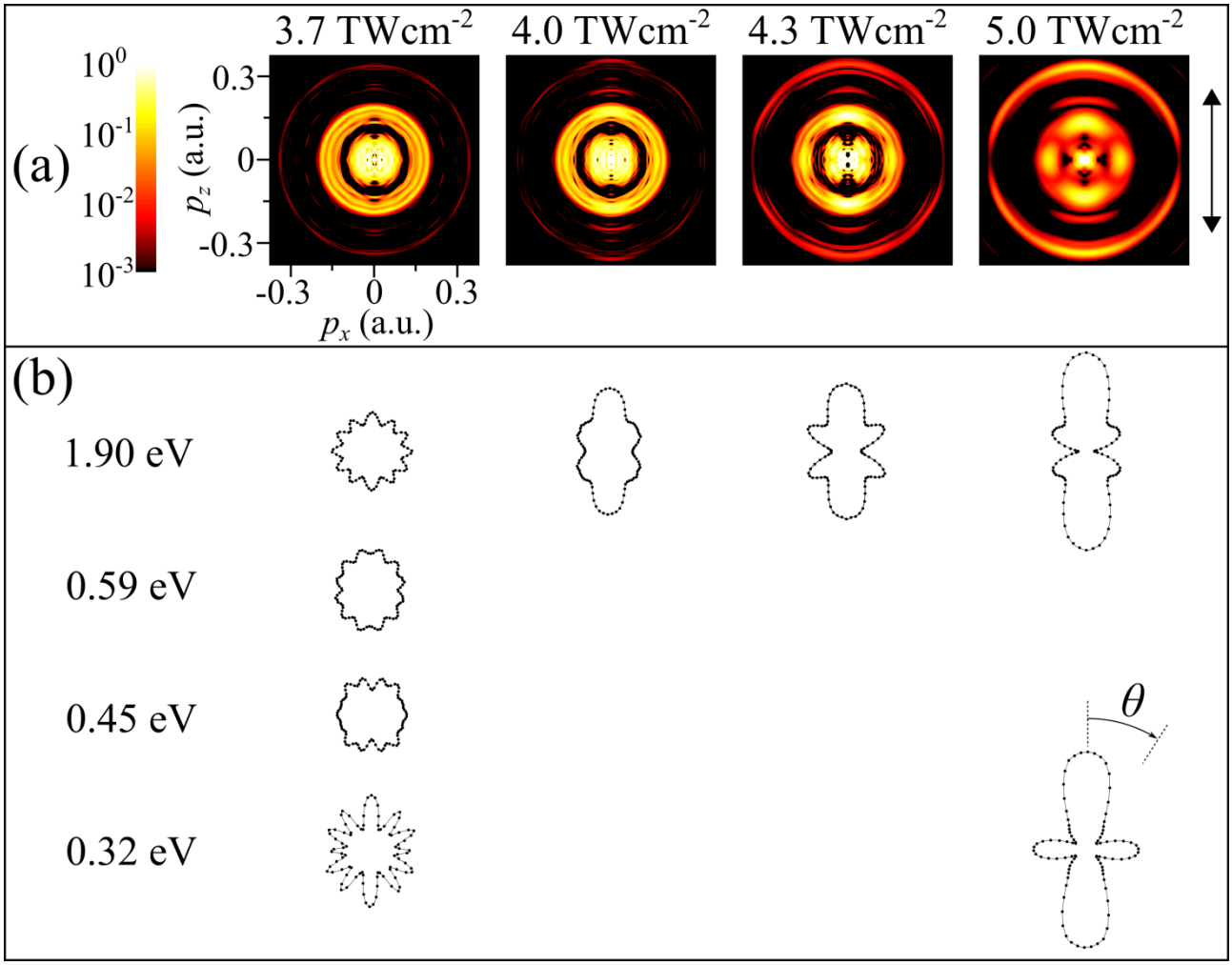

Fig. 6. (a) Inverted (and symmetrized) VMI images recorded at the indicated laser intensities. A logarithmic color scale covering three orders of magnitude is employed for better visibility of their weak features (see the given color bar). The scales of the vertical and horizontal axes are given for a single image but apply to all of them. They are expressed in atomic units of momentum. (b) Normalized polar plots of the PADs obtained from the images in (a) for the indicated electron energies. The evolution of their shapes with intensity and energy is discussed in the text. The angle θ with respect to which the PADs are described is shown in one distribution and it is measured with respect to the linear laser polarization. The direction of the latter is denoted by the black double-headed arrow drawn in (a).

* Current address: Institute of Nanoscience and Nanotechnology, NCSR "Demokritos", Aghia Paraskevi, Athens, Greece.

References

1. I. S. Aleksakhin, I. P. Zapesochnyi, and V. V. Suran, JETP Lett. **26**, 11 (1977); I. S. Alexksakhin, N. B. Delone, I. P. Zapesochnyi, and V. V. Suran, Sov. Phys. JETP **49**, 447 (1979).

2. D. Feldmann, H. J. Krautwald and K. H. Welge, J. Phys. B: At. Mol. Phys., **15**, L529 (1982); D. Feldmann, H. J. Krautwald, S. L. Chin, A. von Hellfeld and K. H. Welge, J. Phys. B: At. Mol. Phys., **15**, 1651 (1982); N. B. Delone, V. V. Suran and B. A. Zon, *Multiphoton Ionization of Atoms*, edited by S.L. Chin and P. Lambropoulos (Academic, New York, 1984); J. L. Dexter, S. M. Jaffe and T. F. Gallagher, J. Phys. B: At. Mol. Phys., **18**, L735 (1985); G. Petite and P. Agostini, J. Phys. (Paris) **47**, 795 (1986); P. Lambropoulos, X. Tang, P. Agostini, G. Petite and Anne L'Huillier, Phys. Rev. A, **38**, 6165 (1988).

3. P. Camus, M. Kompitsas, S. Cohen, C.A. Nicolaides, M. Aymar, M. Crance and P. Pillet, J. Phys. B: At. Mol. Phys., **22**, 445 (1989); Y Zhu, R. R. Jones, W. Sandner, T. F. Gallagher, P. Camus, P. Pillet and J. Boulmer, J. Phys. B: At. Mol. Phys.,**22**, 585 (1989); T. T. Bernat, I. I. Bondar and V. V. Suran, Opt. Spectrosc. **71**, 22 (1991); S. G. Nakhate, S. A. Ahmad, M. A. N. Razvi and G. D. Saksena, J. Phys. B **24**, 4973 (1991); D. A. Tate, D. G. Papaioannou and T. F. Gallagher, J. Phys.B **24** 1953 (1991); D. G. Papaioannou, D. A. Tate and T. F. Gallagher, J. Phys.B **25** 2517 (1992); H. K. Haugen and H. Stapelfeldt, Phys. Rev. A **45**, 1847 (1992); N. J. van Druten, R. Trainham, and H. G. Muller, Phys. Rev. A, **50**, 1593 (1994); I. I. Bondar and V. V. Suran, JETP Lett. **68**, 837 (1998).

4. D. Kim, S. Fournier, M. Saeed and L. F. DiMauro, Phys. Rev. A, **41**, 4966 (1990).

5. P. Lambropoulos, P. Maragakis and J. Zhang, Phys. Rep. **305**, 205 (1998), and references therein.

6. I. I. Bondar, V. V. Suran and M. I. Dudich, J. Phys. B: At. Mol. Phys., **33**, 4243 (2000); I. I. Bondar and V. V. Suran, J. Phys. B: At. Mol. Phys.,**35**, 3391(2002).

7. I. Liontos, A. Bolovinos, S. Cohen, and A. Lyras, Phys. Rev. A, **70**, 033403 (2004); I. Liontos, S. Cohen and A. Lyras, J. Phys. B: At. Mol. Phys., **43,** 095602 (2010).

8. D.I. Bondar, G.L. Yudin, W.K. Liu, M.Y. Ivanov, A.D. Bandrauk, Phys. Rev. A, **83**, 013420 (2011); I.I. Bondar, V.V. Suran, D.I. Bondar, Phys. Rev. A, **88**, 023407 (2013).

9. A. Dimitriou, S. Cohen and A. Lyras, J. Phys. B: At. Mol. Phys., **44,** 135001 (2011); A. Dimitriou, S. Cohen, A. Lyras and I. Liontos, J. Phys. B: At. Mol. Phys., **45**, 205003 (2012).

10. I. Liontos, A. Bolovinos and S. Cohen, J. Phys. B: At. Mol. Phys., **41**, 045601 (2008).

11. A. Dimitriou and S. Cohen*,* Phys. Rev. A, **90**, 012513 (2014).

12. A. Dimitriou and S. Cohen*,* Eur. Phys. J. D, **69**, 238 (2015).

13. *Atoms in Intense Laser Fields*, edited by M. Gavrila, Advances in Atomic, Molecular and Optical Physics, Suppl. 1 (Academic, New York, 1992).
14. L.V. Keldysh, JETP, **20**, 1307 (1965).
15. N. B. Delone and V. P. Krainov, Phys. Usp. **41**, 469 (1998).
16. P. Agostini, F. Fabre, G. Mainfray, G. Petite and N.K. Rahman, Phys. Rev. Lett. **42**, 1127 (1979).
17. M. V. Ammosov, N. B. Delone, M. Yu. Ivanov, I. I. Bondar and A. V. Masalov, Adv. At., Mol., Opt. Phys. **29**, 33 (1991); G. N. Gibson, R. R. Freeman, T. J. McIlrath and H. G. Muller, Phys. Rev. A **49**, 3870 (1994).
18. K. J. Schafer, B. Yang, L. F. DiMauro and K. C. Kulander, Phys. Rev. Lett., **70**,1599 (1993).
19. M. Schuricke, G. Zhu, J. Steinmann, K. Simeonidis, I. Ivanov, A. Kheifets, A. N. Grum-Grzhimailo, K. Bartschat, A. Dorn, and J. Ullrich, Phys. Rev. A, **83**, 023413 (2011).
20. T. Morishita and C. D. Lin, Phys. Rev. A, **87**, 063405 (2013).
21. S.-D Jheng and T. F. Jiang, J. Phys. B: At. Mol. Phys., **46**, 115601 (2013).
22. N. A. Hart, J. Strohaber, A. A. Kolomenskii, G. G. Paulus, D. Bauer, and H. A. Schuessler, Phys. Rev. A, **93**, 063426 (2016).
23. J. Yuan, S. Liu, X. Wang, Z. Shen, Y. Ma, H. Ma, Q. Meng, T.-M. Yan, Y. Zhang, A. Dorn, M. Weidemüller, D. Ye, and Y. Jiang, Phys. Rev. A, **102**, 043112 (2020).
24. D. Zille, D. Adolph, S. Skruszewicz, A. M. Sayler and G. G. Paulus, New J. Phys., **22**, 083021 (2020).
25. P. Wessels, B. Ruff, T. Kroker, A. K. Kazansky, N. M. Kabachnik, K. Sengstock, M. Drescher and J. Simonet, Comm. Phys., **1**, 32 (2018).
26. A. Bunjac, D.B. Popovic, N.S. Simonovic, Physics Letters A, **394**, 127197 (2021).
27. F. Morales, M. Richter, S. Patchkovskii and O. Smirnova, PNAS, **108**, 16906 (2011).
28. M. Aymar, C. H. Greene and E. Luc-Koenig, Rev. Mod. Phys. **68**, 1015 (1996).
29. M. Sukharev, E. Charron and A. Suzor-Weiner, Phys. Rev. A, **66**, 053407 (2002).
30 J. Zhang and P. Lambropoulos, Phys. Rev. Lett. **77**, 2186 (1996).
31. L. Nikolopoulos, G. Buica-Zloh and P. Lambropoulos, Eur. Phys. J. D, **26**, 245 (2003).
32. D. Xenakis, N. E. Karapanagioti, D. Charalambidis, H. Bachau and E. Cormier, Phys. Rev. A, **60**, 3916 (1999).
33. L. D. Van Woerkom, M. J. Nandor, M. A. Walker, G. D. Gillen and H. G. Muller, Laser Physics, **11**, 982 (2001).
34. G. D. Gillen, M. A. Walker and L. D. Van Woerkom, Phys. Rev. A, **64**, 043413 (2001).
35. G. D. Gillen and L. D. Van Woerkom, Phys. Rev. A, **68**, 033401 (2003).

36. E. Papastathopoulos, M. Strehle and G. Gerber, Chem. Phys. Lett., **408**, 65, (2005).

37. H. Kang, S. Chen, Y. L. Wang, W. Chu, J. P. Yao, J. Chen, X. J. Liu, Y. Cheng, and Z. Z. Xu Phys. Rev. A, **100**, 033403 (2019).

38. Y. H. Lai , X. Wang, Y. Li, X. Gong, B. K. Talbert, C. I. Blaga, P. Agostini, and L. F. DiMauro, Phys. Rev. A **101**, 013405 (2020).

39. H. P. Kang, S. Chen, W. Chu, J. P. Yao, J. Chen, X. J. Liu, Y. Cheng, and Z. Z. Xu, Optics Express, **28**, 19325 (2020).

40. A. T. J. B. Eppink and D. H. Parker, Rev. Sci. Instrum. **68**, 3477 (1997).

41. M. M. Harb, S. Cohen, E. Papalazarou, F. Lépine, and C. Bordas, Rev. Sci. Instrum. **81**, 125111 (2010).

42. M. J. J. Vrakking, Rev. Sci. Instrum. **72**, 4084 (2001).

43. K. Zhao, T. Colvin, W. T. Hill and G. Zhang, Rev. Sci. Instrum. **73**, 3044 (2002); G. M. Roberts, J. L. Nixon, J. Lecointre, E. Wrede and J. R. R. Verlet, Rev. Sci. Instrum. **80**, 053104 (2009).

44. A. Talebpour, C.-Y. Chien, Y. Liang, S. Larochelle and S. L. Chin, J. Phys. B: At. Mol. Phys., **30**, 1721 (1997); C. Guo, M. Li, J. P. Nibarger and G. N. Gibson, Phys. Rev. A **5**8, R427 (1998).

45. W. Becker, E. Grasbon, R. Kopold, D. B. Milošević, G. G. Paulus and H. Walther, Advances in Atomic, Molecular and Optical Physics, **48**, 35 (2002).

46. R. R. Freeman, P. H. Bucksbaum, H. Milchberg, S. Darack, D. Schumacher, and M. E. Geusic, Phys. Rev. Lett. **59**, 1092 (1987).

47. Y. Ralchenko, A. Kramida, J. Reader, and NIST ASD Team, 2011 NIST Atomic Spectra Database (version 4.1), http://physics.nist.gov/asd.

48. J. E. Sansonetti and G. Nave, J. Phys. Chem. Ref. Data **39**, 033103 (2010).

49. M. Wollenhaupt, M. Krug, J. Köhler, T. Bayer, C. Sarpe-Tudoran and T. Baumert, Appl. Phys. B **95**, 245 (2009).

50. C. L. Vaillant, M. P. A. Jones and R. M. Potvliege, J. Phys. B: At. Mol. Phys., **47**, 155001 (2014).

51. E. Luc-Koenig, M, Aymar, J.-M. Lecomte and A. Lyras, J. Phys. B: At. Mol. Phys., **31**, 727 (1998).

52. C. C. Chu, H. S. Fung, H. H. Wu and T. S. Yih, J. Phys. B: At. Mol. Phys., **31**, 3843 (1998) and references therein.

53. C. J. Dai and J. Lu, J. Phys. B: At. Mol. Phys., **29**, 2473 (1996).

54. M. Aymar, J.-M. Lecomte, C. C. Chu, H. S. Fung, H. H. Wu and T. S. Yih, J. Phys. B: At. Mol. Phys., **31**, 5135 (1998).

55. L. Hamonou, T. Morishita, and O. I. Tolstikhin, Phys. Rev. A **86**, 013412 (2012).

56. J. Kaur, S. Singh, B. Arora and B. K. Sahoo, Phys. Rev. A **92**, 031402(R) (2015).

57. S. G. Porsev, A. D. Ludlow, M. M. Boyd and J. Ye, Phys. Rev. A **78**, 032508 (2008); K. Guo, G. Wang and A. Ye, J. Phys. B: At. Mol. Phys., **43**, 135004 (2010).

58. S. A. Kotochigova, J. Opt. Soc. Am. B, **9**, 1215 (1992).

59. R. M. Potvliege and S. Vučić, Physica Scripta, **74**, C55 (2006).

60. E. Mevel, P. Breger, R. Trainham, G. Petite, and P. Agostini, Phys. Rev. Lett., **70**, 406 (1993).

61. H. R. Reiss, Phys. Rev. Lett. **101**, 043002 (2008); Erratum: Phys. Rev. Lett. **101**, 159901 (2008).

62. K. D. Schultz , C. I. Blaga, R. Chirla, P.Colosimo, J. Cryan, A. M. March, C. Roedig, E. Sistrunk, J. Tate, J. Wheeler, P. Agostini and L. F. DiMauro, J. Mod. Opt., **54**, 1075 (2007); P. Agostini and L. F. DiMauro, Advances in Atomic Molecular and Optical Physics, **61**, 117 (2012); L. F. DiMauro and C. A. Roedig, Progress in Ultrafast Intense Lase Science, X, Springer Series in Chemical Physics 106, Chapter 5, 65-76 (2014).

63. M. Goto and K. Hansen, Phys. Scr. **86**, 035303 (2012).

64. B. Witzel, N. A. Papadogiannis and D. Charalambidis, Phys. Rev. Lett., **85**, 2268 (2000); B. Witzel et al, Nuclear Physics A**737** 306 (2004).

65. K. Amini, J. Biegert, F. Calegari and A. Chacón, Rep. Prog. Phys. **82**, 116001 (2019).

66. G. D. Borisova et al, J. Phys. Commun. **4**, 055012 (2020).